A&A, 707, A211 (2026)
https://doi.org/10.1051/0004-6361/202558396

Astronomy & Astrophysics

The gas-phase nitridation processes of large, astronomically relevant polycyclic aromatic hydrocarbons cations in the interstellar medium

Congcong Zhang[1,⋆], Yanan Ge[2], Ziyi Wang[1], Wei Wang[1], Lijun Hua[1], Nian Zhao[1], Xuejuan Yang[1,⋆], and Junfeng Zhen[1]

[1] Hunan Key Laboratory for Stellar and Interstellar Physics and School of Physics and Optoelectronics, Xiangtan University, Xiangtan, Hunan 411105, China
[2] National Key Laboratory of Deep Space Exploration/School of Earth and Space Sciences, University of Science and Technology of China, Anhui, Hefei 230026, China

Received 4 December 2025 / Accepted 27 January 2026

ABSTRACT

Atomic nitrogen reacts efficiently with polycyclic aromatic hydrocarbons species, and potentially generates a diverse array of complex organic molecules in the interstellar medium. In this work, the gas-phase chemical evolution of large, astronomically relevant PAH, tetra-benzo-pero-pyrene (TBPP, $C_{36}H_{16}$) cations under N-atom bombardment is investigated experimentally and theoretically. A series of nitridated TBPP cations, including $[C_{36}H_{16}N_n]^+$ (n=1–5) and dehydrogenated species $[C_{36}H_{10-15}N_n]^+$ (n=1–5), are effectively formed. Additionally, we identify denitridation pathways of nitridated TBPP cations that, through loss of a CN or HCN/HNC unit, lead to the formation of smaller PAH cations (with odd carbon numbers and five-membered carbon cycles, e.g., $[C_{35}H_{15}]^+$). We investigated the structures and the vibrational infrared spectra of newly formed nitridated TBPP cations and the bonding energy for the reaction pathways using theoretical calculations, which were based on density functional theory with the hybrid density functional B3LYP/6-311++G(d, p). The reaction energy is relatively high, which indicates that the addition of N atoms to the carbon skeleton is a random and independent event, i.e., there is no carbon-edge structural effect. Furthermore, theoretical analyses confirm that denitridation pathways involving the loss of CN or HCN/HNC units are energetically favorable, which underscores their potential role in the top-down evolution of large PAHs. The obtained results highlight the importance of PAH cations evolution under N-atom bombardment, and demonstrate the formation of complex organic species containing nitrogen functionalities, such as C=N, C–N–H, and C–N–C groups. Furthermore, these findings provide insights into the molecular diversity and chemical evolution of PAHs, where ion-atom collisions drive both the functionalization and structural truncation of large molecules in astrophysical environments.

Key words. astrochemistry – molecular processes – methods: laboratory: molecular – ISM: clouds – ISM: molecules

1. Introduction

The existence of polycyclic aromatic hydrocarbons (PAHs) in the interstellar medium (ISM) is well supported by the widespread detection of unidentified infrared (UIR) emission bands at wavelengths of 3.3, 6.2, 7.7, 8.6, 11.2, 12.7, and 16.4 μm across numerous Galactic and extra-galactic sources (Gillett et al. 1973; Cohen et al. 1986; Allamandola et al. 1989; Tielens 2013; Li 2020). These spectral features are generally attributed to the infrared fluorescence of large PAH molecules (~50–100 C atoms), mainly following excitation by ultraviolet (UV) photons (Leger & Puget 1984; Allamandola et al. 1985, 1989). These observed infrared fluorescences are also referred to as aromatic infrared bands (AIBs) (Tielens 2013, and references therein). Variations in the peak positions, widths, and relative intensities of the AIBs have been observed, which can reflect the physical and chemical differences in the local ISM conditions (Hony et al. 2001; Peeters et al. 2002; Sakon et al. 2004). In addition, such spectral diversity implies the presence of a (highly) heterogeneous population of PAH species (Vats et al. 2022, and references therein).

Polycyclic aromatic hydrocarbons can be further processed for a hundred million years in the harsh environment of the ISM. Observational and laboratory studies have indicated that a substantial fraction of these PAH species predominantly reside in dense molecular clouds (Snow & Bierbaum 2008; Cernicharo et al. 2021, 2023, 2026, and references therein), including a wide variety of PAHs with functional groups, such as methyl (-CH_3), vinyl (-$CHCH_2$), methoxy (-OCH_3), amino (-NH_2), cyano/isocyano (-CN, -NC), acid (-COOH), and hydroxyl (-OH) (Joblin et al. 1996; Geballe et al. 2011; Yang et al. 2020). The presence of nitrogen-functionalized PAHs is an interesting subject due to their potential role in explaining key astronomical observations and their relevance to prebiotic chemistry (Hudgins et al. 2005; Mattioda et al. 2017).

Nitrogen, ranked as the fifth most abundant universal element (Snow & Bierbaum 2008), exists predominantly in its atomic form (N I) within diffuse interstellar regions (Meyer et al. 1997). Hubble Space Telescope spectrograph observations of the N (^{2}P)1160, 1161 absorption doublet yield a mean interstellar gas-phase abundance (per 10^6 H atom) of 10^6 N/H=75 ± 4 (±1σ),

⋆ Corresponding authors: zhangcongcong@xtu.edu.cn; xjyang@xtu.edu.cn

which indicates a present-day Galactic abundance that is approximately 80% of the Solar System value (Meyer et al. 1997). In the dense and cold environments of molecular clouds, chemical models and observational studies agree that the dominant reservoir of nitrogen is atomic nitrogen, rather than molecular nitrogen (Viala 1986; Womack et al. 1992; Maret et al. 2006; Daranlot et al. 2012; Kruczkiewicz et al. 2021). This is mainly due to the inefficiency of the N_2 gas-phase formation pathways under typical dark cloud conditions, which leads to a significant portion of elemental nitrogen depleting onto dust grains and potentially forming ices like NH_3 (Daranlot et al. 2012).

Polycyclic aromatic nitrogen heterocycles (PANHs) could constitute another reservoir of nitrogen in the Universe, in addition to nitrogen in the gas phase and ices of the ISM. PANHs are considered important prebiotic precursors and have been detected in meteoritic organic matter (Yang et al. 2020). Importantly, recent radio astronomical detections of nitrogen-functionalized naphthalene derivatives and aromatic hydrocarbon indene in a dense molecular cloud further reinforce the significance of N-containing PAHs in space (McGuire et al. 2021; Cernicharo et al. 2021, 2023, 2026, and references therein). Cernicharo et al. (2023) and Cernicharo et al. (2026) reported the first interstellar detection of benzonitrile (C_6H_5CN) and 3- and 4-cyano isomers of acenaphthylene ($C_{12}H_8$), which possibly formed through bottom-up chemical processes, in the cold dark cloud TMC-1, based on observations from the Yebes 40m radio telescope. These findings highlight the prevalence of complex organic structures in astrophysical environments and the role of nitrogen incorporation in expanding the chemical diversity of interstellar molecules (Rap et al. 2022).

In astrophysical environments, the formation and evolution of nitrogen-bearing organic compounds are governed by a complex interplay of thermal reactions, photochemical processes, and radiation-induced chemistry (Cryan et al. 2025). These species are produced through various pathways, including ion-molecule interactions (e.g., N^+ reactions with hydrocarbons like benzene Ascenzi et al. 2001), radical-radical associations (Balucani et al. 2015), and likely through the degradation of complex refractory organic materials, such as those found in cometary grains or meteoroids (Pisarčíková et al. 2023; Fray et al. 2005). Nitrogen-atom endohedral fullerenes ($N@C_{60}$) have been synthesized in the sublimation phase (Cho et al. 2015), and their physical properties, including electronic structures, have been computationally studied (Lu & Zhao 1999; Kobayashi & Dinse 2003; Plakhutin et al. 2005). The specific formation route and survival of these molecules are highly sensitive to local conditions (Bakes & Tielens 1994; Le Page et al. 2001), such as temperature, UV radiation fields, and the presence of shocks (Zhang et al. 2023b). Consequently, the observed abundances and isomeric ratios of N-bearing molecules (e.g., HCN, HNC, HC_3N, $N@C_{60}$) serve as powerful diagnostic tools for probing the physical and chemical histories of diverse environments, from cold dark clouds and protostellar regions to cometary comae and planetary atmospheres (Balucani et al. 2015; Fray et al. 2005). By tracing the incorporation of nitrogen into molecular form, these compounds provide a critical observational framework for understanding nitrogen's evolution in space (Zhang et al. 2023b).

In this work, we investigate gas-phase reactions between tetra-benzo-pero-pyrene (TBPP, $C_{36}H_{16}$) cations and nitrogen atoms to elucidate the chemical evolutionary processes of large, astrophysically relevant PAHs with N atoms in the interstellar environments. TBPP ($C_{36}H_{16}$, 36 C-atoms, m/z=448), within the size range of astrophysical PAHs, serves as a prototypical model for large(r) aromatic species (Andrews et al. 2015; Croiset et al. 2016). The molecular geometry of TBPP is illustrated in Figure 1, where distinct edge structures – solo (red), duo (blue), and trio (yellow) – are highlighted to facilitate an analysis of edge-specific effects on the nitridation pathways. We conducted experimental investigations using an apparatus equipped with a quadrupole ion trap and a reflection time-of-flight mass spectrometer (see Appendix A for details). We used a free microplasma source to generate N atoms at a flux of $\sim 10^{12}$ N atom cm^{-2} s^{-1}. We performed complementary quantum chemistry calculations (detailed in Appendix B) to characterize the nitridated molecular structures, reaction mechanisms, and corresponding infrared (IR) spectral features.

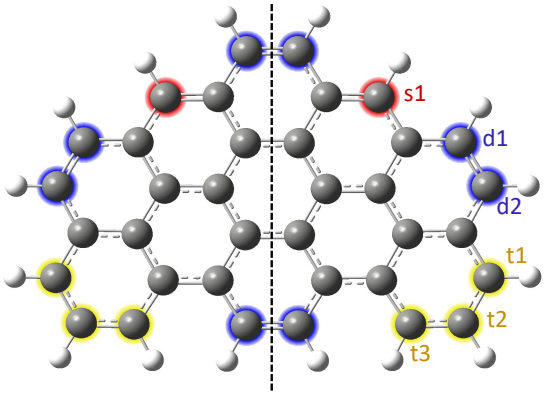

Fig. 1. Molecular geometry of tetra-benzo-pero-pyrene (TBPP, $C_{36}H_{16}$).

2. Experimental results

Figure 2 presents the mass spectrum of nitridated TBPP cations ($[C_{36}H_{16}N_n]^+$) in the m/z range of 392–546. As shown in Fig. 2A, when the exposure time of the N-atom (2.0, 5.0, and 10.0 s) is increased, the mass spectrum shows a progressive shift in the mass distribution toward higher m/z values. This formation behavior suggests nitrogen atoms are progressively added to TBPP cations, which confirms the efficiency of the nitridation processes. Figure 2B, which is a magnified view of the mass spectrum at 10.0 s of exposure time, resolves distinct peaks corresponding to nitridated species $[C_{36}H_{16}N_n]^+$ (n=1–5). Notably, the highest-mass cations observed at m/z=518 are assigned to $[C_{36}H_{16}N_5]^+$, which demonstrates that five nitrogen atoms have been incorporated into PAH molecules by sequential additions of N atoms.

In addition to TBPP cations ($[C_{36}H_{16}]^+$, m/z=448), Figure 2 reveals the presence of dehydrogenated TBPP (DTBPP) cations ($[C_{36}H_{10-15}]^+$, m/z=442–447), which are generated via electron impact ionization and fragmentation of TBPP (Zhen 2019). Similarly, nitridated DTBPP species ($[C_{36}H_{10-15}N_n]^+$, n=1–5) are observed in Figure 2B. Interestingly, DTBPP cations exhibit heightened chemical reactivity compared to their nondehydrogenated counterparts. For instance, $[C_{36}H_{14}N]^+$ displays a peak intensity comparable to $[C_{36}H_{16}N]^+$, while $[C_{36}H_{14/15}N_2]^+$ shows a higher intensity than $[C_{36}H_{16}N_2]^+$. This enhanced reactivity may be attributed to the presence of dehydrogenated peripheral carbon sites in DTBPP cations, which provide favorable reaction sites for the addition (Zhang et al. 2023a).

Regarding the nitridation reaction pathways, similarly to our previous work on the oxygenation processes of PAH cations

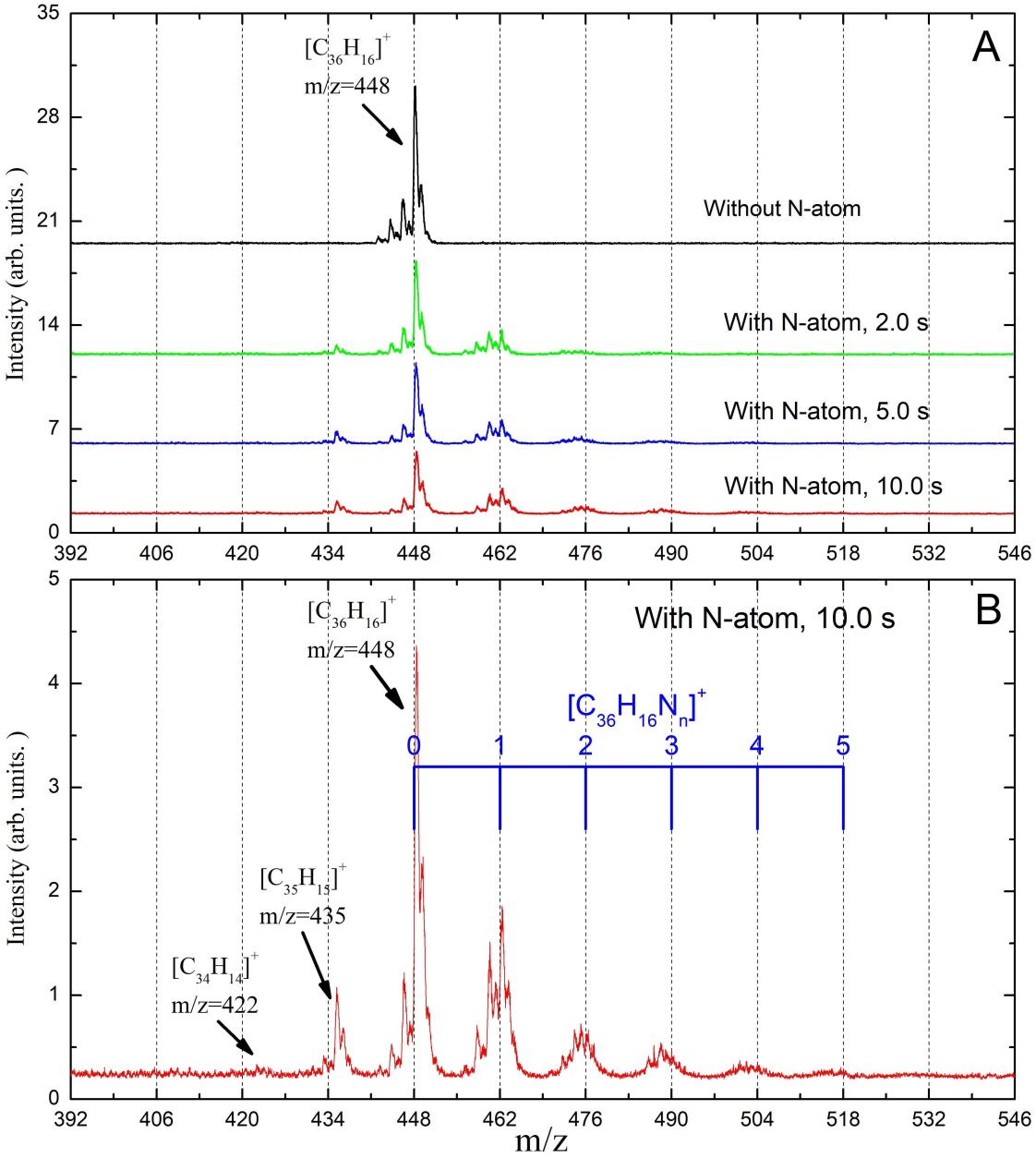

Fig. 2. Panel A: evolution mass spectra of TBPP cations with different N atom exposure times (2.0, 5.0, and 10.0 s); Panel B: zoomed in mass spectrum (10.0 s) that reveals the presence of $[C_{36}H_{10-16}N_n]^+$ and $[C_{35}H_{15}]^+$, $[C_{34}H_{14}]^+$ in detail.

(Hu et al. 2025), we suppose that the formation of nitridated (D)TBPP cations arises from ion-atom collision reactions between (D)TBPP cations and atomic nitrogen. These reactions proceed through sequential addition mechanisms, where nitrogen atoms are incorporated via repeated collisional events. Based on that, the nitridation pathways for the resulting nitridated (D)TBPP cations are summarized as

$$[C_{36}H_{10-16}N_n]^+ + N \longrightarrow [C_{36}H_{10-16}N_{n+1}]^+, \quad n = [0, 4].$$

Intriguingly, Figure 2B reveals two additional mass peaks at m/z=435 ($[C_{35}H_{15}]^+$) and m/z=422 ($[C_{34}H_{14}]^+$), which we attribute to truncated TNPP cations. These species likely arise from denitridation processes of nitridated TBPP cations, which are analogous to the collision- or photo-induced deoxidation pathways observed in oxidized PAH cations (Hu et al. 2025), where HCO/CO units are sequentially lost. Specifically, we propose that $[C_{35}H_{15}]^+$ and $[C_{34}H_{14}]^+$ originate from nitridated TBPP cations through the elimination of CN or HCN/HNC units. However, unlike the clear observation of deoxidation intermediates in Hu et al. (2025), we cannot resolve nitridated derivatives due to isotopic interference. For instance, the mass peak of $[C_{35}H_{15}N]^+$ at m/z=449 overlaps with the isotopic tail of TBPP ($[^{13}C^{12}C_{35}H_{16}]^+$), which has an identical nominal mass.

The denitridation of nitridated (D)TBPP cations is proposed to proceed through two interconnected mechanisms: (1) sequential nitrogen atom additions followed by the elimination of CN or HCN/HNC units, and (2) energy-driven fragmentation enabled by internal energy accumulated from prior exothermic nitridation reactions (Hu et al. 2025). Drawing from these insights, the denitridation pathways for nitridated (D)TBPP cations are

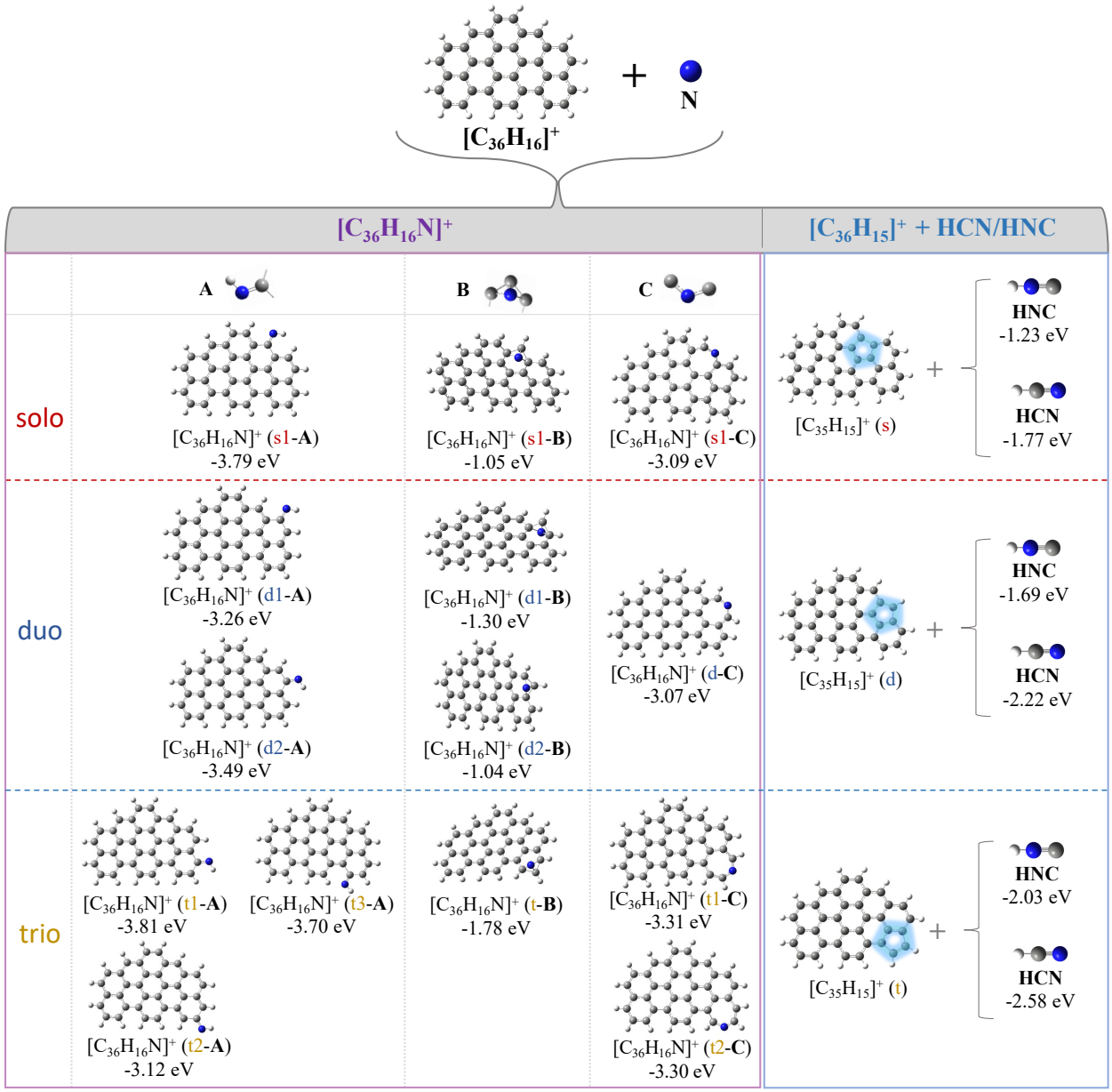

Fig. 3. Theoretical calculation results for the reaction pathways of $[C_{36}H_{16}]^+$ and N atoms.

summarized as

$$[C_{36}H_{16}]^+ + N \longrightarrow [C_{35}H_{15}]^+ + HNC/HCN$$
$$[C_{36}H_{15}]^+ + N \longrightarrow [C_{35}H_{15}]^+ + CN.$$

Overall, the efficient formation of nitridated (D)TBPP cations is primarily driven by ion-atom collision reactions between (D)TBPP cations and atomic nitrogen. The denitridation pathways have been identified, which involve the elimination of CN or HCN/HNC units from nitridated (D)TBPP cations. Together with the calculation results, we discuss the observed experimental results in the next section.

3. Quantum calculation results

To elucidate the nitridation mechanisms of large PAHs, we conducted quantum-chemical calculations of the reaction pathways for the reaction between (D)TBPP cations and atomic nitrogen. Specifically, the reaction systems studied include $[C_{36}H_{16}]^+ + N$ and $[C_{36}H_{15}]^+ + N$, respectively. Figure 1 illustrates the molecular geometry of $C_{36}H_{16}$. We chose TBPP because it displays solo, duo, and trio peripheral carbon sites, with a size in the astrophysically relevant range.

To evaluate the influence of these structural motifs on the reaction energetics, we selected one group of representative sites from each category (solo, duo, trio) for detailed chemical analysis (labeled as s1, d1, d2, t1, t2, and t3 in Fig. 1). For the cationic systems (e.g., $[C_{36}H_{16}]^+$ and $[C_{36}H_{15}]^+$), we adopted doublet spin multiplicity. For N atoms, we considered the quartet spin multiplicity (^4S).

3.1. The reaction pathways of $[C_{36}H_{16}]^+ + N$

The calculated results for the reaction pathways of $[C_{36}H_{16}]^+ + N$, are presented in Figure 3. We obtained two groups of different

reaction patterns: the first is $[C_{36}H_{16}]^+ + N \rightarrow [C_{36}H_{16}N]^+$ and the second is $[C_{36}H_{16}]^+ + N \rightarrow [C_{35}H_{15}]^+ + HCN/HNC$.

For the first group of reaction patterns, $[C_{36}H_{16}]^+ + N \rightarrow [C_{36}H_{16}N]^+$, the optimized structures of the nitridated products are categorized into three structural types based on the resulting C-N bonding motifs (shown in the vertical panels in Figure 3). The formation of $[C_{36}H_{16}N]^+$ isomers involves the creation of: C-N-H functional groups at peripheral carbon sites (Type A), multi-C-N bridge bonds across three adjacent carbon atoms (Type B), or C-N-C functional groups via C-C bond cleavage (Type C). We considered and obtained 14 reaction pathways, and the reaction energies for these pathways range from −3.12 to −3.81 eV (Type A), −1.04 to −1.78 eV (Type B), and −3.07 to −3.31 eV (Type C), respectively. The high exothermicity of Type A and C pathways suggests a strong thermodynamic favorability for the formation of C-N-H and C-N-C bonds, whereas the less exothermic Type B pathways indicate lower reactivity for multisite bonding. In particular, for trio edge structures, the side carbon atoms (t1, t3) exhibit an exothermicity of ∼0.7 eV. This is higher than that of the middle carbon atom (t2) and highlights their higher chemical activity. These findings imply that laboratory-formed $[C_{36}H_{16}N]^+$ is likely a mixture of isomers, with Type A and C products dominating due to their thermodynamic preference.

For the second group of reaction patterns, $[C_{36}H_{16}]^+ + N \rightarrow [C_{35}H_{15}]^+ + HCN/HNC$, smaller fragments of TBPP ($[C_{35}H_{15}]^+$) are newly formed through elimination of HCN/HNC. This process, characterized by reaction energies ranging from −1.23 to −2.58 eV, confirms its thermodynamic feasibility. The resulting $[C_{35}H_{15}]^+$ (s/d/t) fragments originate from the loss of HCN or HNC units, with structural variations arising from the formation of five-membered carbon rings at different edge sites (solo, duo, and trio). The reaction energy is different between the formation of HNC and HCN pathways; for example, the reaction energy is −1.23 eV for $[C_{36}H_{16}]^+ + N \rightarrow [C_{35}H_{15}]^+$ (s) + HNC, and the reaction energy is -1.77 eV for $[C_{36}H_{16}]^+ + N \rightarrow [C_{35}H_{15}]^+$ (s) + HCN. While the energy released during the denitrification process is comparable for HCN/HNC loss pathways, which suggests similar thermodynamic probabilities for the formation of either unit, the associated fragmentation mechanisms are kinetically constrained by their multistep nature, which entails C-C bond cleavage and ring formation. Previous studies suggest that such processes likely involve multiple transition states or transient intermediates; the intermolecular hydrogen transfer processes also play an important role (de Haas et al. 2017; West et al. 2018; Hu et al. 2025). However, such kinetic mechanisms were not explicitly accounted for in our current theoretical study. This underscores the necessity of further theoretical investigations to clarify the detailed energy barriers and hydrogen migration dynamics in these processes.

3.2. The reaction pathways of $[C_{36}H_{15}]^+ + N$

As illustrated in Figure 4, the molecular geometry of dehydrogenated TBPP (DTBPP, $[C_{36}H_{15}]^+$) reveals six distinct isomers based on the structural configurations of outer carbon edge sites (solo, duo, and trio). We systematically investigated the nitridation processes of each isomer, and categorized the reaction pathways between $[C_{36}H_{15}]^+$ and nitrogen atoms into two different patterns: $C_{36}H_{15}^+ + N \rightarrow [C_{36}H_{15}N]^+$ and $C_{36}H_{15}^+ + N \rightarrow [C_{35}H_{15}]^+ + CN$.

For the first group, the optimized structures of $[C_{36}H_{15}N]^+$ products, presented in the vertical panels of Figure 4 (left), show the formation of C–N functional groups at dehydrogenated

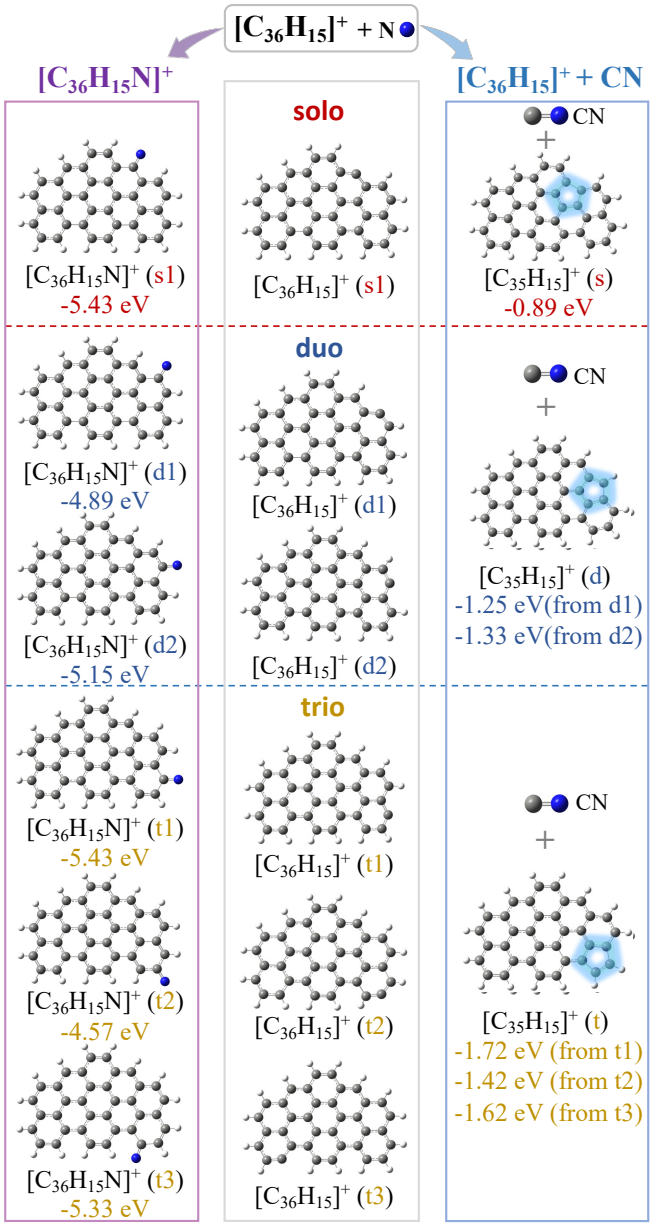

Fig. 4. Theoretical calculation results for the reaction pathways of $[C_{36}H_{15}]^+$ and N atoms.

outer-carbon sites. The reaction energies range from −4.57 to −5.43 eV, higher than those observed for TBPP cations (−3.12 to −3.81 eV). This enhanced exothermicity suggests that DTBPP cations exhibit higher chemical reactivity with N atoms compared to their nondehydrogenated counterparts. The thermodynamic favorability of these pathways implies that $[C_{36}H_{15}N]^+$ formed in laboratory experiments is likely to be a mixture of isomers arising from the diverse edge-site geometries of DTBPP.

The second group involves the formation of smaller PAH fragments ($[C_{35}H_{15}]^+$) through CN unit elimination, as in $[C_{36}H_{15}]^+ + N \rightarrow [C_{35}H_{15}]^+ + CN$. The reaction energies for this process range from −0.89 to −1.72 eV, which indicates thermodynamic feasibility but lower exothermicity compared to direct nitridation. The resulting $[C_{35}H_{15}]^+$ (s/d/t) fragments originate from the loss of CN units, with structural variations arising from the formation of five-membered carbon rings at different edge sites (solo, duo, and trio). For example, the reaction

$[C_{36}H_{15}]^+$ (d1) + N → $[C_{35}H_{15}]^+$ (d) + CN has a reaction energy of −1.25 eV, while $[C_{36}H_{15}]^+$ (d2) + N → $[C_{35}H_{15}]^+$ (d) + CN yields −1.33 eV, demonstrating subtle pathway-specific differences. However, the complexity of CN loss channels, similar to HCN/HNC loss channels in Section 3.1, which involve multistep mechanisms such as C–C bond cleavage and ring formation, as well as intermolecular hydrogen transfer processes (de Haas et al. 2017; West et al. 2018; Hu et al. 2025), necessitates further theoretical investigations.

3.3. Discussion

The obtained theoretical calculations align closely with the experimental results. This consistency confirms that the gas-phase collision reaction between (D)TBPP cations and nitrogen atoms proceeds readily, yielding multiple reaction pathways and a diverse array of nitridated PAHs (N-PAHs). The different nitridation bonding motifs result in the formation of various nitrogen-containing functional groups (e.g., C=N, C-N-H, and C-N-C). The computational results indicate that the reaction energies of nitridation pathways at different carbon sites are comparable. Notably, the carbon skeleton structure, particularly peripheral edge features, exerts a negligible influence on the nitridation processes of (D)TBPP cations. This suggests that nitrogen incorporation into the carbon skeleton of $[C_{36}H_{16}]^+$ is a relatively independent event.

In particular, smaller TBPP PAHs, such as $[C_{35}H_{15}]^+$, are newly formed. These molecules, which possess an odd number of carbon atoms and five-membered carbon cycles (e.g., 35 C-atoms), are generated via the top-down fragmentation route. Furthermore, the enhanced exothermicity of nitridation of dehydrogenated TBPP cations (compared to TBPP) confirms the role of dehydrogenation in promoting nitrogen incorporation, while the loss pathways for CN or HCN/HNC units illustrate the potential for defunctionalization to smaller, structurally modified PAHs. We observe that the molecules can overcome these activation barriers because they retain significant internal energy from prior exothermic steps in the proposed mechanism, thereby enabling the top-down fragmentation route.

3.4. IR spectra of nitridated (D)TBPP cations

The newly formed nitridated PAH cations identified in this study are potential candidates for the observed interstellar IR bands. These species may originate in the same interstellar region through a coevolving ion-molecular reaction network involving PAHs and nitrogen atoms. N-PAHs could contribute to the interstellar spectrum and motivate further spectroscopic investigations (Tielens 2013). Figure 5 presents the calculated IR spectra of representative nitridated TBPP cations in the 0–3500 cm^{-1} range. Panel (A) corresponds to $[C_{36}H_{16}]^+$; panels (B1-E1) depict A-type $[C_{36}H_{16}N]^+$ isomers (s1-A, d1-A, t1-A, and t2-A); panels (F1-H1) show C-type $[C_{36}H_{16}N]^+$ isomers (s1-C, d-C, and t1-C); panels (B2-C2) illustrate B-type $[C_{36}H_{16}N]^+$ isomers (d1-B and t-B); panels (D2-F2) display $[C_{35}H_{15}]^+$ isomers (s, d, and t); and panels (G2-H2) correspond to $[C_{36}H_{15}N]^+$ isomers (s1 and t1).

The IR spectra shown in Figure 5 exhibit significant complexity. Overall, the IR spectra of the parent TBPP cations and their nitridated derivatives show a marked similarity. Some new vibration modes are formed, and the vibrational peaks vary within a small range because of the influence of local structural morphing. The emergence of new vibrational modes and the observed spectral complexity demonstrate the structural diversity of these molecules and the intricate interplay of functional groups within their carbon skeletons. Among the features observed, only one characteristic vibration mode is clearly identifiable: a single peak at ∼3306 cm^{-1}, assigned to N-H stretching vibrations. However, the C=N stretching modes (∼1529–1594 cm^{-1}) and C-N stretching vibrations (∼1193–1267 cm^{-1}) are obscured due to a strong overlap with the vibrational peaks associated with C-C and C=C bonds. Additionally, a distinct (N)C-H stretching mode is observed in the 2992–3041 cm^{-1} range that differs from the typical C-H stretching vibrations of PAHs.

4. Astronomical implications

The origin and evolution of large molecules (e.g., PAHs and fullerenes) in space represent a significant topic of scientific interest. The presence of these large molecules has been proposed to account for key features observed in interstellar IR spectra (Tielens 2013). PAHs exhibit complex spatial distributions and undergo intricate molecular and structural evolution in interstellar environments. These molecules are influenced by a range of environmental factors, including interstellar UV radiation, metallicity, atomic density, and interactions with coexisting species (Tielens 2013; Zhang et al. 2025), which drive their evolution across distinct evolving phases in the ISM. This study presents the first comprehensive demonstration of the chemical evolution of PAH molecules under nitrogen-atom bombardment, analyzed from multiple perspectives.

A series of nitridated PAH cations ($[C_{36}H_{16}N_n]^+$ with n=[1–5]) and nitridated dehydrogenated PAH cations ($[C_{36}H_{10-15}N_n]^+$ with n=[1–5]) are efficiently generated by gas-phase ion-atom collision reactions between PAH cations and nitrogen atoms. The formation of highly nitridated species such as $[C_{36}H_{16}N_5]^+$ indicates that the nitridation processes of PAH cations are favorable, allowing efficient production of nitridated PAH cations in the interstellar gas-phase environments. Our theoretical calculations indicate that these nitridation reactions are exothermic and have high reaction energies. The nitridation process appears stochastic and unconstrained, and lacks site-specific preferences for PAH species. As a result, the resulting nitridation states and configurations of PAH derivatives exhibit substantial diversity and complexity.

According to the obtained theoretical calculation results, losing CN or HCN/HNC units from nitridated species is a thermodynamically favorable pathway, which aligns with experimental results of collision-induced denitrification of nitridated PAHs. This denitrification process results in the formation of PAH derivatives possessing an odd number of carbon atoms (e.g., 35 C atoms) and incorporating five-membered carbon rings. It is important to note, however, that our present theoretical study does not encompass all the potential reaction pathways. Particularly when the number of N-atom added to TBPP is high, additional intramolecular interactions and other pathways may emerge. Furthermore, the multistep fragmentation pathways, which entail carbon-carbon bond cleavage and subsequent ring formation, involve kinetic barriers that were not explicitly accounted for in our current theoretical study.

Importantly, aside from the photo-driven denitrification of nitridated PAH cations in the ISM, collision reaction-induced denitrification is also expected to participate in the top-down evolution routes of large PAHs. Considering the relatively high interstellar fluxes of H/D, C, and O atoms, as well as other coexisting molecules, nitridated PAHs will frequently interact with these coexisting species. Such collision reactions could

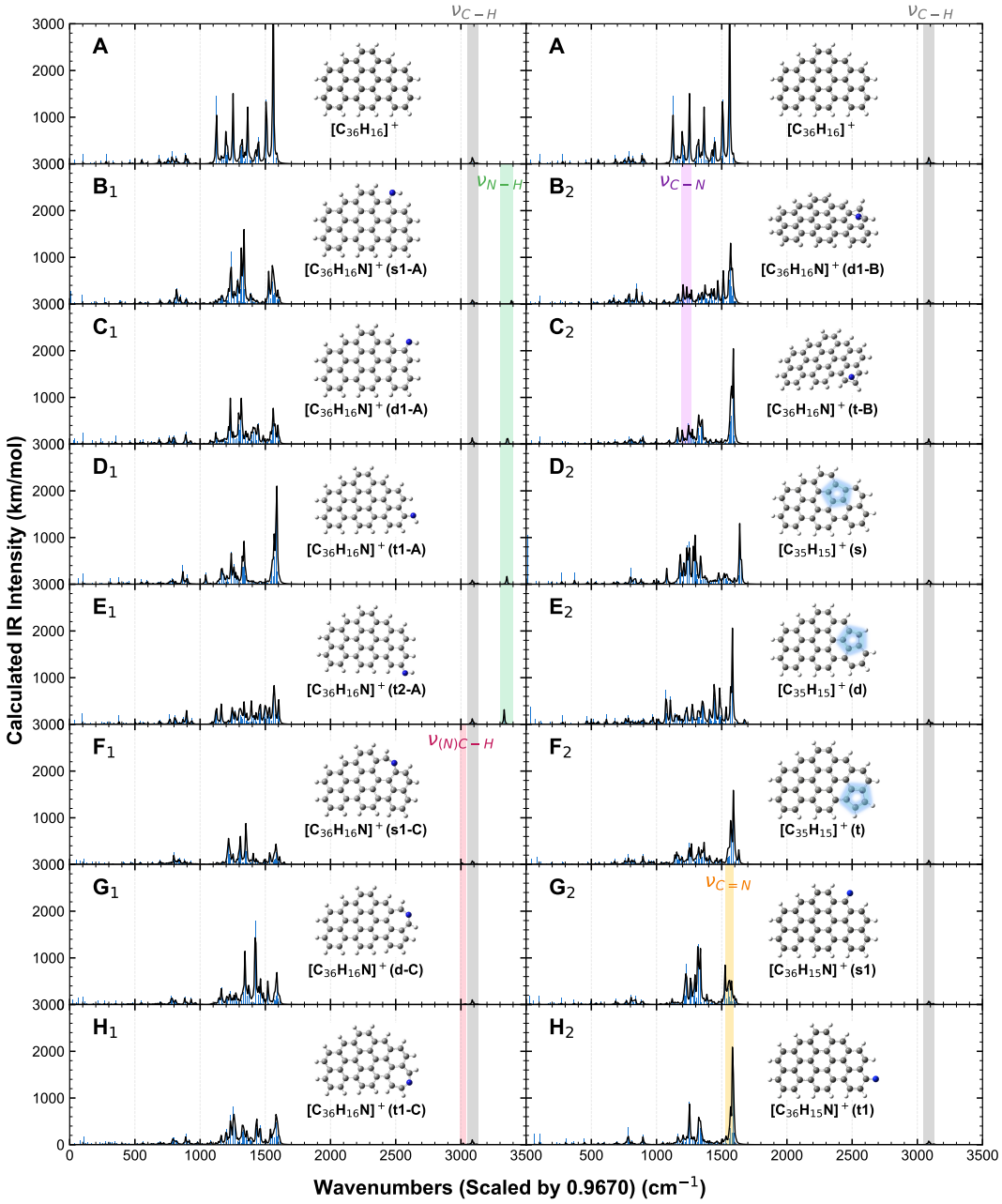

Fig. 5. Computed vibrational normal modes are represented: Panel (A) for $[C_{36}H_{16}]^+$; panels (B1-E1) for A-type of $[C_{36}H_{16}N]^+$ (s1-A, d1-A, t1-A, and t2-A); panels (F1-H1) for C-type of $[C_{36}H_{16}N]^+$ (s1-C, d-C, and t1-C); panels (B2-C2) for B-type of $[C_{36}H_{16}N]^+$ (d1-B and t-B); panels (D2-F2) for $[C_{35}H_{15}]^+$ (s, d, and t); and panels (G2-H2) for $[C_{36}H_{15}N]^+$ (s1 and t1).

promote more efficient denitrification or lead to the formation of more complex organic molecules in the interstellar environment (Hu et al. 2025). The dynamic interplay between nitrogen incorporation and elimination pathways (resulting in both larger, nitrogen-functionalized PAHs and smaller, truncated fragments) provides critical insights into the molecular evolution of PAHs in astrophysical environments. These processes not only shape the structural diversity of interstellar PAHs but also influence their spectroscopic signatures, such as UV absorption and IR emission features, which are essential for interpreting observational data.

In brief, the ion-atom reaction mechanisms observed in laboratory experiments can be considered analogous to gas-phase collision pathways between PAH cations and nitrogen atoms in the ISM. These findings align with the broader picture of PAH evolution in astrophysical settings, where ion-atom collisions drive both functionalization and structural truncation, and contribute to the observed molecular diversity and spectroscopic signatures of interstellar PAHs. The molecular spectra derived from the computed structures of nitridated PAH cations exhibit significant diversity and complexity. Vibrational modes involving nitrogen atoms display distinct characteristics due to variations in bond types (e.g., C-N-H, C-N, and C=N) and their local structural morphing. These findings necessitate careful interpretation of the interstellar IR spectrum, which emphasizes the need for approaches aligned with more intricate molecular derivatives.

To demonstrate the feasibility of identifying key spectral features, Figure 6 overlays the calculated IR spectra of selected

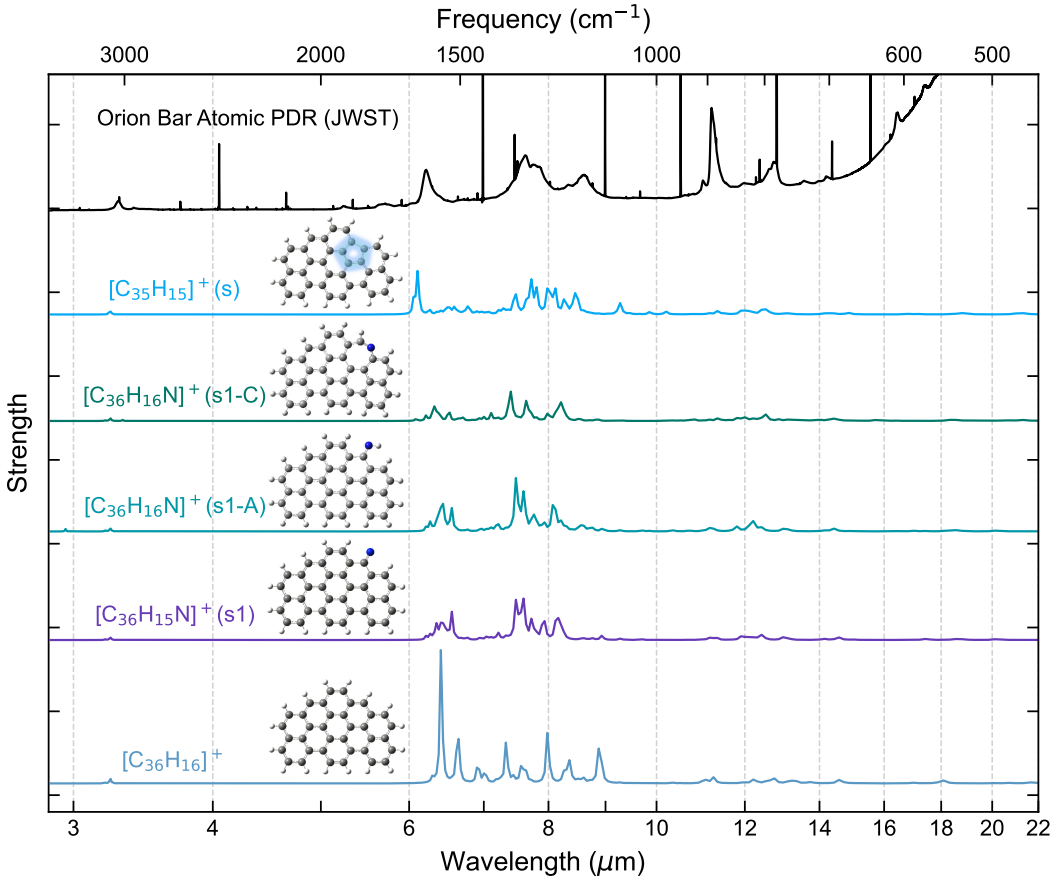

Fig. 6. Obtained IR spectra of some typical nitridated TBPP cations. These are replotted together with a representative observed spectrum. The observed spectrum is a representative interstellar IR spectrum observed by JWST (Chown et al. 2024; Peeters et al. 2024). The observed spectrum includes typical AIBs extracted from the atomic PDRs of the Orion Bar.

nitridated TBPP cations with a representative interstellar IR spectrum observed by the James Webb Space Telescope (JWST) (Chown et al. 2024; Peeters et al. 2024). The observed spectrum (black line, Fig. 6) includes typical AIBs that are extracted from the atomic photodissociation region (PDR) of the Orion Bar. This spectrum reveals a possible partial similarity to the calculated IR profiles of nitridated TBPP cations. However, there are notable discrepancies in specific wavelength ranges, which complicate the identification of characteristic vibrational peaks associated with distinct nitrogen-containing functional groups. These results stressed the challenges in correlating theoretically calculated spectra with interstellar observations, particularly because vibrational modes overlap and are influenced by the environmental factors.

5. Conclusions

Our combined experimental and theoretical investigations present the chemical evolution of large PAH cations under nitrogen atom bombardment. Through gas-phase condensation and fragmentation processes, PAH cations undergo structural transformations that may lead to increasingly complex molecular architectures. The present results suggest that nitrogen incorporation likely plays a significant role in shaping the chemical diversity of interstellar PAHs and is consistent with a high level of structural complexity for PAHs in space. This complexity may arise from the interplay of environmental factors (such as ion-atom collisions, dehydrogenation, and radical-mediated reactions) that can drive both functionalization and defunctionalization pathways.

By examining the thermodynamics and mechanisms of potential nitrogen-driven reactions, our work aims to provide a framework for understanding how PAHs could contribute to the synthesis of complex organic molecules in space. Such insights may aid in the interpretation of observational signatures (such as infrared emission features) and in exploring the astrochemical pathways that might influence the evolution of carbon-rich matter in the universe.

Acknowledgements. This work was supported by the National Natural Science Foundation of China (NSFC, Grant No. 12333005).

References

Ascenzi, D., Franceschi, P., Freegarde, T. G. M., et al. 2001, Chem. Phys. Lett., 346, 35
Allamandola, L. J., Tielens, A. G. G. M., & Barker, J. R. 1985, ApJ, 290, L25
Allamandola, L. J., Tielens, A. G. G. M., & Barker, J. R. 1989, ApJS, 71, 733
Andrews, H., Boersma, C., Werner, M. W., et al. 2015, ApJ, 807, 99
Bakes, E. L. O., & Tielens, A. G. G. M. 1994, ApJ, 427, 822
Balucani, N., Leonori, F., Petrucci, R., et al. 2015, Chem. Phys., 449, 34
Becke, A. D. 1992, JChPh, 96, 2155
Boersma, C., Bauschlicher Jr., C. W., Ricca, A., et al. 2014, ApJS, 211, 8
Cernicharo, J., Agúndez, M., Cabezas, C., et al. 2021, A&A, 649, L15
Cernicharo, J., Tercero, B., Marcelino, N., et al. 2023, A&A, 674, L4
Cernicharo, J., Tercero, B., Marcelino, N., et al. 2026, A&A, 705, L7

Cho, S. C., Kaneko, T., Ishida, H., & Hatakeyama, H. 2015, J. Appl. Phys. 117, 123301
Chown, R., Sidhu, A., Peeters, E., et al. 2024, A&A, 685, A75
Cohen, M., Allamandola, L., Tielens, A. G. G. M., et al. 1986, ApJ, 302, 737
Croiset, B. A., Candian, A., Berné, O., & Tielens, A. G. G. M. 2016, A&A, 590, A26
Cryan, S., Brunetto, R., Guilbert-Lepoutre, A., et al. 2025, EPSC-DPS Joint Meeting 2025
Daranlot, J., Hincelin, U., Bergeat, A., et al. 2012, Proc. Natl. Acad. Sci. USA, 109, 10233
de Haas, A. J., Oomens, J., & nitri, J. 2019, Phys. Chem. Chem. Phys., 19, 2974
Fray, N., Bénilan, Y., Cottin, H., et al. 2005, Planet. Space Sci., 53, 1243
Frisch, M. J., Trucks, G. W., Schlegel, H. B., et al. 2016, Gaussian 16, Revision e. 01 Wallingford, CT: Gaussian, Inc.
Geballe, T. R., Najarro, F., Figer, D. F., Schlegelmilch, B. W. & de La Fuente, D. 2011, Nature, 479, 200
Gillett, F. C., Forrest, W. J., & Merrill, K. M. 1973, ApJ, 183, 87
Grimme, S., Ehrlich, S., & Goerigk, L. 2011, JCoCh, 32, 1456
Hony, S., Van Kerckhoven, C., Peeters, E., et al. 2001, A&A, 370, 1030
Hu, X., Zhao, N., Zhang, C., et al. 2025, ApJ, 980, 195
Hudgins, D. M., Bauschlicher, C. W., & Allamandola, L. J. 2005, ApJ, 632, 316
Joblin, C., Tielens, A. G. G. M., Allamandola, L. J., & Geballe, T. R. 1996, ApJ, 458, 610
Kobayashi, K., Nagase, S., & Dinse, K. P. 2003, Chem. Phys. Lett., 377, 93
Kruczkiewicz, F., Vitorino, J., Congiu, E., et al. 2021, A&A, 652, A29
Lee, C., Yang, W., & Parr, R. G. 1988, PhRvB, 37, 785
Le Page, V., Snow, T. P., & Bierbaum, V. M. 2001, ApJS, 132, 233
Leger, A., & Puget, J. L. 1984, A&A, 137, L5
Li, A. 2020, Nat. Astron., 4, 339
Lu, J., Zhang, X., & Zhao, X. 1999, Chem. Phys. Lett., 312, 85
Maret, S., Bergin, E. A., & Lada, C. J. 2006, Nature, 442, 425
Mattioda, A. L., Bauschlicher, C. W., Ricca, A., et al. 2017, Spectrochim. Acta Part A Mol. Spectr., 181, 286
McGuire, B. A., Loomis, R. A., Burkhardt, A. M., et al. 2021, Science, 371, 1265
Meyer, D. M., Cardelli, J. A., & Sofia, U. J. 1997, ApJ, 490, L103
Peeters, E., Hony, S., Van Kerckhoven, C., et al. 2002, A&A, 390, 1089
Peeters, E., Habart, E., Berné, O., et al. 2024, A&A, 685, A74
Pisarčíková, A., Matlovič, P., Tóth, J., et al. 2023, Icarus, 404, 115682
Plakhutin, B. N., Breslavskaya, N. N., Gorelik, E. V., & Arbuznikov, A. V. 2005, JMoSt, 727, 149
Rap, D. B., Schrauwen, J. G. M., Marimuthu, A. N., et al. 2022, Nat. Astron., 6, 1059
Sakon, I., Onaka, T., Ishihara, D., et al. 2004, ApJ, 609, 203
Snow, T. P., & Bierbaum, V. M. 2008, Annu. Rev. Anal. Chem., 1, 229
Tielens, A. G. G. M. 2013, RvMP, 85, 1021
Vats, A., Pathak, A., Onaka, T., et al. 2022, PASJ, 74, 161
Viala, Y. P. 1986, Astron. Astrophys. Suppl. Ser., 64, 391
West, B., Castillo, S. R., Sit, A., et al. 2018, Phys. Chem. Chem. Phys., 20, 7195
Womack, M., Ziruys, L. M., & Wyckoff, S. 1992a, ApJ, 387, 417
Yang, Y., Hu, X., Zhang, D., et al. 2020, MNRAS, 498, 1
Zhang, C., Hu, X., Ge, Y., et al. 2023a, A&A, 669, A41
Zhang, X., Quan, D., Li, R., et al. 2023b, MNRAS, 521, 1578
Zhang, C., Hales, J., Peeters, E., et al. 2025, ApJS, 280, 1
Zhen, J. 2019, A&A, 623, A102

Appendix A: Experimental methods

The experiments were conducted using a quadrupole ion trap (QIT) coupled to a reflection time-of-flight mass spectrometer (ReTOF-MS). Briefly, neutral tetra-benzo-pero-pyrene (TBPP, $C_{36}H_{16}$) was converted into a gas by heating its powdered form (provided by Kentax, with a purity greater than 99.5 %) in an oven (~ 450 K). The evaporated TBPP molecules were subsequently ionized and transported into the ion trap via an ion gate. During this procedure, helium gas was introduced continuously into the trap via a leaking valve to thermalize the ion cloud through collisions (~ 300 K).

A Free Microplasma Source (FMP, MBE-Komponenten GmbH) was employed to generate N atoms via a localized plasma at its tip. Ultra-high-purity N_2 gas (>99.99 %) served as the precursor for this process. The chamber pressure during plasma working was ~ 3.0×10^{-6} mbar (the background pressure was ~ 3.0×10^{-7} mbar, realized with helium gas). The working parameters of FMP: the RF power is 8.0 W; the operation frequency is 2464 MHz; the PD intensity is 62 a.u.; the gas flow of N_2 is 0.3 SCCM; the TC temperature is 390 K. According to the FMP manual, an N/N_2 ratio of 2.6 was determined, corresponding to a predicted flux of N atom of ~ 10^{12} N atom cm^{-2} s^{-1} and a volume density of ~ 10^7 cm^{-3}; The separation distance between the FWP tip terminus and the ion trap center was ~ 3.0 cm. The nitrogen atom was directed into the ion trap through a 2.4 mm aperture in the ring electrode.

A high-precision digital delay/pulse generator (SRS, DG535) provided precise timing control with the following parameters: Our setup was operated with a frequency of 0.5, 0.2, or 0.1 Hz, i.e., one complete measuring cycle lasted 2.0, 5.0, or 10.0 s, respectively. During each experimental cycle, the ion gate was opened to accumulate a certain amount of ions within the trap. Then nitridated TBPP cations formed, and adduct formation presumably occurred. In the final step, a negative square pulse was applied to the end cap, the ions were extracted from the trap and transferred to the mass spectrometer for detection, and the resulting mass fragments were measured.

Appendix B: Quantum chemistry calculation methods

Theoretical calculations were carried out based on density functional theory with the hybrid density functional B3LYP (Becke 1992; Lee et al. 1988), as implemented in the Gaussian 16 program (Frisch et al. 2016). The 6-311++G(d, p) basis set was used throughout the system. In addition, dispersion correction (D3) was considered to account for intermolecular interactions (Grimme et al. 2011). The geometries of all species were optimized at the local minimum of their potential energy surface. The zero-point energy and thermal corrections obtained from the frequency calculation were used to correct the molecular energy.

The vibrational spectra of these nitridated PAH cations were computed at the B3LYP/6-311++G(d, p) level of theory. The positions of the vibrational bands were scaled by a constant factor of 0.9670, and the spectra were simulated by Gaussians with a full width at half maximum of 4 cm^{-1} (Boersma et al. 2014).